Molecular Crystals and Liquid Crystals Science and Technology. Section A. Molecular Crystals and Liquid Crystals

Publication details, including instructions for authors and subscription information:
http://www.tandfonline.com/loi/gmcl19

Silica Dispersed Nematics and Cholesterics for Bistable High Resolution Displays

M. Bittner [a] & M. Kreuzer [a]

[a] Institute of Applied Physics, Technische Hochschule, Darmstadt, Germany

Version of record first published: 24 Sep 2006.

To cite this article: M. Bittner & M. Kreuzer (1996): Silica Dispersed Nematics and Cholesterics for Bistable High Resolution Displays, Molecular Crystals and Liquid Crystals Science and Technology. Section A. Molecular Crystals and Liquid Crystals, 282:1, 373-386

To link to this article: http://dx.doi.org/10.1080/10587259608037591

Mol. Cryst. Liq. Cryst., 1996, Vol. 282, pp. 373–386
Reprints available directly from the publisher
Photocopying permitted by license only

SILICA DISPERSED NEMATICS AND CHOLESTERICS FOR BISTABLE HIGH RESOLUTION DISPLAYS

M. BITTNER and M. KREUZER
Institute of Applied Physics, Technische Hochschule Darmstadt, Germany

Abstract Highly dispersed silica forms a rebuildable network in nematics capable of stabilizing domains of different optical properties. Displays with silica dispersed (or *filled*) nematics can be laser-addressed to a scattering state, allowing high resolution display applications as well as optical data storage.
A theory based on nematodynamics identifies the laser writing process as a thermal shock effect and corresponds well with experimental results. With this knowledge, the sensitivity of the material was improved using small amounts of chiral dopants. It is also shown that silica dispersed cholesterics with pitch lengths in the visible range form bistable cholesteric textures (BCT). These filled cholesterics can be laser-addressed to a focal conic transparent state or to a reflecting state, depending on the surface treatment of the cell plates.

INTRODUCTION

Dispersions of pyrogenic silica (AEROSIL™, by Degussa AG) in nematics have been known for a few years as materials for bistable laser-addressed scattering displays[1]. The cells allow bistable switching between a transparent state (by applying a short voltage pulse) and a scattering state (by writing with a focused laser beam). A diluted dye usually serves to enhance the absorption of laser energy.

In contrast to other thermally addressed displays[2], no phase transition is involved in this laser writing, so that displays with Filled Nematics (FN) can operate over a wide temperature range. Also, no special liquid crystal material is required and cells are easy to fabricate. The displays offer intrinsic high resolution, good contrast, high lumen yield (no polarizers needed) and continuous grey scale. The storage of images with 4096 × 4096 pixels has been demonstrated[3].

To show the excellent suitability of FN for high resolution large-scale projection systems, we have built a demonstration unit which was presented at the 1995 CeBIT exhibition. Fig. 1 gives a schematic view of this system: The collimated beam of a diode laser ($\lambda = 780\,\text{nm}$) is deflected by two galvanometer scanners and writes an image onto the display, which is projected on-line to a screen. Some of the features are a resolution of 2000 × 2000 pixels, a writing speed of ca. 200 lines/s and contrast ratios in excess of 50:1 (with f/2.8 objective) for filled chiral nematics.

For further investigations and improvements on the electro-optical and all-optical properties of the material it is very important to understand the physical mechanism of laser writing, since experiments have shown that the generation of the scattering state is *not* due to a nematic-isotropic phase transition. We have developed a model based on the hydrodynamics of nematics which is in good accordance with our experiments.

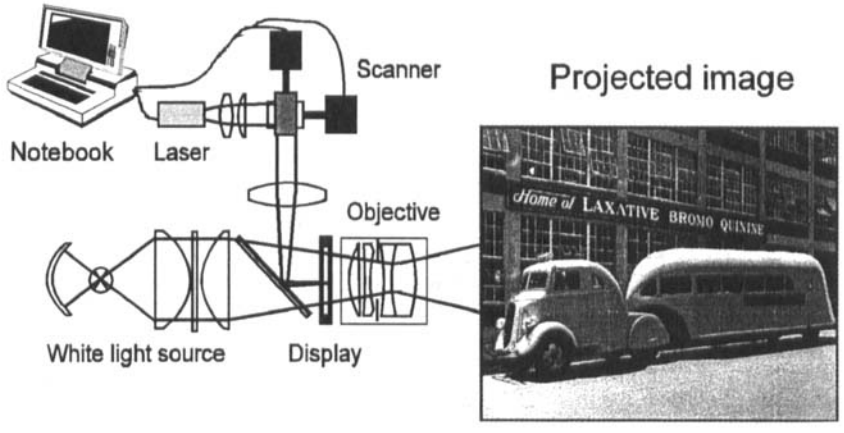

Figure 1: Schematic view of the demonstration unit

MATERIAL

The small volume fraction (1..3%) of dispersed silica does not influence the bulk optical properties of the LC, but forms an open network which divides the nematic in domains of different orientation. The large specific surface (up to 380 m^2/g) of Aerosil with several possible interactions at the LC-Aerosil interface can be seen here as a random field acting on the liquid crystal molecules.

Aerosil consists of spherical primary particles of SiO_2 (diameter 12 nm for type R974), which form chain-like aggregates via Si-O-Si bonds.Through SiOH groups at the surface (0.5..2.5 per nm^2), the aggregates can form larger agglomerates and build up an open network stabilized by hydrogen bonds. Transmission electron microscopy of such an Aerosil network yields an average domain size of about 250 nm.

The material is sandwiched between ITO-coated glass plates , typically with 14 μm glass fiber spacers. After preparation, such a cell is in a scattering state due to the optical anisotropy of the liquid crystal which forms randomly aligned nematic domains.

By applying a certain voltage to a FN cell, a transparent homeotropic state can be created that remains stable when the electric field has been removed. Since it can be shown that there is strong anchoring of the LC molecules at the Aerosil surface, LC reorientation leads to a torque on the solid structure which is sufficient to break up hydrogen bonds connecting the agglomerates[3]. After this process, the transparent state is stabilized by the formation of a new network.

In the following section, we explain why FN cells can be locally written to a strongly scattering state with a laser beam.

THEORY OF LASER WRITING

For a description of the laser action on Filled Nematics, the FN layer is simplified as a system of randomly orientated capillaries filled with nematic liquid crystal, as shown in Fig. 2a. The domain size of the real material is chosen as the capillary diameter l_m. The effects of laser exposure may be described as follows:

First, laser energy is absorbed by the diluted dye leading to a very rapid increase in temperature and thus to a change in density. Since the volume expansion coefficient of the LC is much larger than that of the Aerosil structure, a hydrodynamic flow of LC in the capillaries occurs. Fig. 2b shows a single capillary orientated parallel to the cell plates, with homeotropic LC orientation. Because of the strong anchoring at the capillary walls, laser exposure will cause a flow with a velocity profile as shown. Since the Reynolds number of this flow is very small ($Re << 1$), it will be a laminar Poiseuille flow which makes the LC molecules reorientate from their initial homeotropic state. It also causes shear forces acting on the capillary walls which can break up hydrogen bonds that connect the Aerosil agglomerates. After the laser pulse, the solid structure can form again and stabilize the new scattering state.

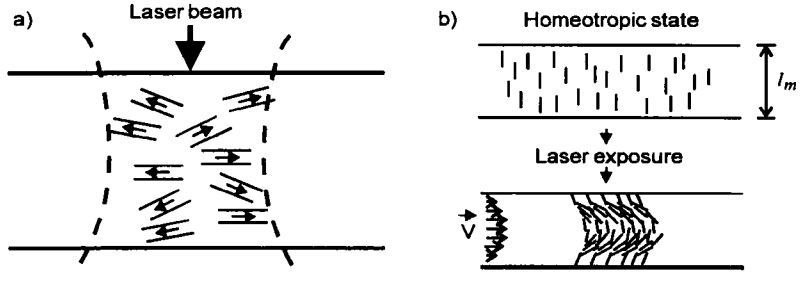

Figure 2: a) Capillary model; laser exposure induces hydrodynamic flow of NLC.
b) Flow and reorientation in a single capillary.

The following treatment of this effect uses conventional hydrodynamics (Navier-Stokes-Equation for compressible media) as well as nematodynamics (the coupling of flow and reorientation)[4]. Also, heat diffusion in the layer and mass conservation (continuity equation) have to be taken into account. For simplification, all tensor material constants are replaced by effective scalar quantities.

Basic equations

The following four equations have to be considered to describe the model system[5]:

$$\frac{\partial T}{\partial t} = r_t \Delta T + \frac{W}{V \rho_o C_p} \tag{1}$$

$$\frac{\partial^2 \rho}{\partial t^2} = \tilde{c}^2 \Delta \rho + \eta \frac{\partial}{\partial t} \rho + \rho_o \tilde{c}^2 \alpha \Delta T \tag{2}$$

$$\frac{\partial \rho}{\partial t} = -\mathrm{div} \rho v \tag{3}$$

$$\gamma_1 \frac{\partial \Theta}{\partial t} = K \Delta \Theta - \frac{1}{2}\left(\gamma_1 - \gamma_2 \cos 2\Theta\right) \frac{\partial v_z}{\partial x} \tag{4}$$

with the parameters r_t: heat conductivity , W: absorbed laser power in volume V, C_p: heat capacitance, ρ_o: density, $\tilde{c}$: speed of sound, η: viscosity, K: Frank elastic constant and $\gamma_1 = \alpha_3 - \alpha_2, \gamma_2 = \alpha_6 - \alpha_5$, α_i: Leslie coefficients.

To analyze these equations, it is very instructive to find typical time constants. In the following, we assume an incident Gaussian beam with the intensity distribution

$$I = I_o \cdot \exp\left(\frac{-2r^2}{\omega_o^2}\right) . \tag{5}$$

Eq. (1) describes heat diffusion in the FN layer and its time constant can be estimated as

$$\tau_{therm} = \frac{1}{2r_t}\left(\frac{1}{\omega_o^2} + \frac{1}{D^2}\right)^{-1} \tag{6}$$

with ω_o: laser beam waist and D: cell thickness.

Eq. (4) accounts for reorientation of the nematic director in the flow. A time constant can be estimated with

$$\tau_{dir} = \frac{\gamma_1 l_m^2}{4K\pi^2} . \tag{7}$$

Eq. (2) for the density distribution is derived from the Navier-Stokes equation. Its analytical solution[5] for a laser pulse of duration $\tau_p < \tau_{therm}$ gives the density development during laser exposure ($t < \tau_p$):

$$\rho(r,t) = \rho_o - t\frac{FI\sigma}{\rho_o C_p \tilde{c}^2}\left\{\exp\left\{-\frac{2r^2}{\omega_o^2}\right\} + S(r,t)\right\} \quad \text{for } t \le \tau_p \tag{8}$$

with

$$S(r,t) = \frac{\pi^2 \omega_o^2 \tilde{\eta}}{2\tilde{c}^2 t}\left[\mathrm{Ei}\left(-\frac{\pi^2 r^2}{s_2^2}\right) - \mathrm{Ei}\left(-\frac{\pi^2 r^2}{s_1^2}\right)\right] , \tag{9}$$

$$s_1^2 = \tfrac{\omega_o^2 \pi^2}{2} , \qquad s_2^2 = \tfrac{\omega_o^2 \pi^2}{2} + \tfrac{\tilde{c}^2 t}{\tilde{\eta}} , \qquad -\mathrm{Ei}(-z) = \int_z^\infty u^{-1} e^{-u} \mathrm{d}u$$

and $\quad F = \rho_o \tilde{c}^2 \alpha , \quad \tilde{\eta} = \tfrac{2\pi^2 \eta}{l_m^2} , \quad \sigma :$ absorption $[\mathrm{cm}^{-1}]$.

The change in density consists of two terms: The first is a Gaussian function – with an amplitude increasing linearly with time – which resembles the equilibrium distribution for the temperature at a given time t. The second term describes a decreasing perturbation $S(r,t)$ from the Gaussian distribution which is rather strong due to the large viscosity of the material.

A calculation based on the Fourier transform of Eq. (2)[5] yields the time constant τ_ρ of the perturbation:

$$\tau_\rho = \frac{4\pi^4 \eta \omega_o^2}{l_m^2 \tilde{c}^2} \ . \tag{10}$$

Optimum writing conditions

With all time constants, we can define a condition for the optimum conversion of absorbed laser energy into LC reorientation for a laser pulse of length τ_p:

$$\tau_\rho < \tau_p < \min(\tau_{dir}, \tau_{therm}) \tag{11}$$

assuring that during laser exposure ($t < \tau_p$) the equilibrium value for the density change is reached ($\tau_p > \tau_\rho$), whereas no energy is lost due to heat diffusion ($\tau_p < \tau_{therm}$) and reorientation does not reach saturation ($\tau_p < \tau_{dir}$). Fig. 3 visualizes the optimum writing conditions, with the time constants being calculated using typical values for the material constants.

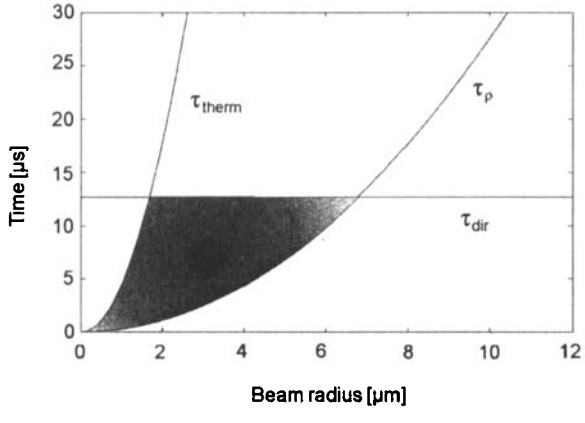

Figure 3: Optimum writing conditions: The hatched area marks the range for the laser pulse duration τ_p and the beam size ω_o where inequality (11) holds.

Reorientation

If condition (11) is fulfilled, the density distribution may be estimated with the time-dependent equilibrium distribution:

$$\rho(r,t) \approx -\frac{FI\sigma}{\rho_o C_p \tilde{c}^2} t \exp\left\{-\frac{2r^2}{\omega_o^2}\right\} + \rho_o \quad \text{for } t \leq \tau_p \ . \tag{12}$$

Inserting $\rho(r,t)$ in the continuity equation (3), the flow velocity can be calculated:

$$v_o(r) = \frac{FI\sigma\pi^2\omega_o^2}{16\rho_o^2 C_p \tilde{c}^2}\left\{\frac{1}{r}\left[1-\exp\left(-\frac{2r^2}{\omega_o^2}\right)\right]\right\} . \tag{13}$$

When the director equation (4) is linearized using the appproximation $\gamma_1 \approx -\gamma_2$:

$$\gamma_1\frac{\partial\Theta}{\partial t} - K\Delta\Theta + \gamma_1\frac{\partial v}{\partial x} = 0 , \tag{14}$$

the reorientation angle Θ_o becomes

$$\Theta_o \approx \Theta_{max}\left(1-\exp\left\{-\frac{t}{\tau_{dir}}\right\}\right) \tag{15}$$

with

$$\Theta_{max} = \frac{\gamma_1 l_m v_{o,max}}{4K\pi} \approx \frac{0.9}{64}\frac{\gamma_1 l_m \pi\sigma\alpha}{K\rho_o C_p \omega_o}P . \tag{16}$$

Therefore the maximum scattering contrast (which is assumed proportional to the maximum reorientation Θ_{max}) should be a linear function of the laser *power* P, not of the laser pulse energy $P \cdot \tau_p$. This result points out the thermal shock nature of the writing process.

One expects a saturation of contrast with increasing reorientation angle Θ_o; of course there is also an absolute maximum $\Theta_{max,s}$ for reorientation predicted by Eq. (4):

$$\Theta_{max,s} = 90° - \frac{1}{2}\arccos\left|\frac{\gamma_1}{\gamma_2}\right| . \tag{17}$$

EXPERIMENTS

Various experiments – of which we will show two examples here – have been carried out to prove these theoretical predictions.

The first experiment is concerned with the dynamical behaviour of the induced flow. When the optimum writing conditions are violated by a large beam waist ω_o in combination with low laser power, the change in density does not reach its equilibrium value during the laser exposure. So one should be able to detect the temporal development of the induced flow by monitoring the contrast for different times of exposure. The time constant of these curves should be equal to τ_ρ, which can thus be measured as a function of the laser beam radius ω_o. It is important to state here that the time of exposure was always shorter than the time constant for heat diffusion

$$\tau_p < \tau_{therm},$$

so that the result cannot be confused with a thermal effect, which has a similar dependence on the beam radius.

To measure τ_ρ, we recorded the scattering contrast vs. time of exposure τ_p for variable waist ω_o of the focused beam. An experimental setup similar to Fig. 1

was used. The writing speed was controlled by a function generator connected with one of the scanners, providing a constant laser exposure time τ_p for the written spots. The focus diameter (mimimum spot size: $\approx 10\mu$m) was varied by shifting the display in the direction of the laser beam. A small area was written on the display and projected on the sensor area of a photodiode recording the transmitted intensity.

The values of τ_ρ for all beam sizes are plotted in the double logarithmic diagram of Fig. 4. They are in good accordance with the theoretical result $\tau_\rho \propto \omega_o^2$ (Eq. 10) marked by the straight line. This proves our assumptions about the laser-induced hydrodynamic flow.

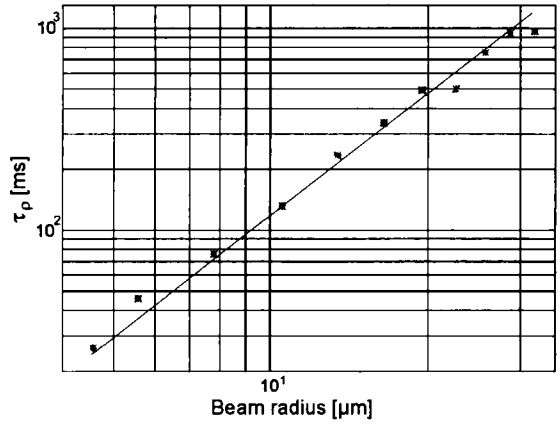

Figure 4: Double logarithmic plot of the measured time constants τ_ρ vs. beam radius ω_o. The straight line marks the theoretical result $\tau_\rho \propto \omega_o^2$.

The second experiment is concerned with the thermal shock nature of the writing process. We measured the maximum achievable contrast as a function of laser power. Here the time of exposure was increased at fixed laser power until the contrast reached its maximum value; this was done for different values of the laser power.

The result is shown in Fig. 5. The maximum contrast is proportional to the laser power P (as predicted by Eq. 16) for a certain range until it reaches a saturation value. The linear behaviour also justifies the assumption that contrast is a linear function of reorientation.

So both experiments show a very good agreement with the theoretical predictions. For applications, one of the most important points is the sensitivity, which can be defined as the absorbed energy per area needed to reach a certain contrast value. We assume a reorientation angle of $\Theta_o = 60°$ for a good contrast and calculate

$$s = \frac{\text{absorbed energy } E}{\text{area } A} = \frac{P\tau_p}{\pi\omega_o^2} \approx 0.7\frac{\text{nJ}}{\mu\text{m}^2}$$

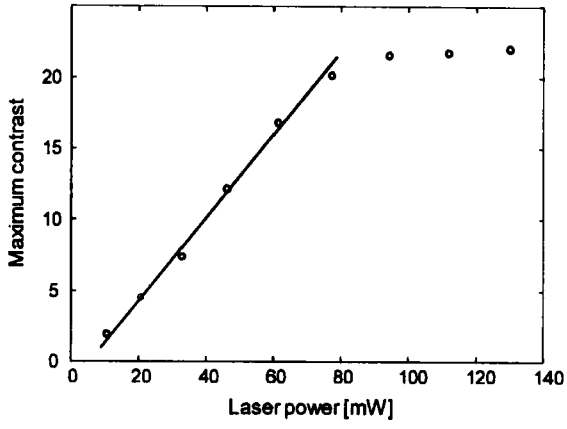

Figure 5: The maximum contrast is a linear function of laser *power* until saturation is reached.

in good agreement with experimental values s=0.5..1.5 nJ/μm^2.

IMPROVING THE SENSITIVITY

From the theoretical model, we can estimate the magnitude of the torque density produced by shear forces in the hydrodynamic flow:

$$\tau = \frac{\eta \cdot \rho \cdot v_{o,max}}{l_m} \approx 10^3 \frac{\mathrm{J}}{\mathrm{m}^3} \tag{18}$$

But from thixotropy experiments – which measure the viscosity change of silica dispersed liquids in a shear flow – the energy density of hydrogen bonds in the Aerosil structure can be approximated as

$$\Gamma_{OH} \approx 10^2 \frac{\mathrm{J}}{\mathrm{m}^3} \tag{19}$$

so that only a small fraction of the laser energy is needed to destabilize the network, whereas the main part serves to reorientate the LC molecules. Therefore, it seems reasonable to provide some means of storing energy in the transparent state of a FN cell. This was achieved by adding chiral dopants to the nematic: Applying an electric field can unwind the cholesteric helix leading to a homeotropic state stabilized by the Aerosil network. So elastic energy of deformation can be stored in a transparent cell, which should be set free during the laser writing process.

However, the pitch energy density should not be larger than the energy density of the Aerosil hydrogen bonds, because this could prevent obtaining a stable homeotropic state. To determine the maximum concentration of chiral dopants experimentally, we recorded the electro-optical behaviour of different filled chiral nematics. The pitch length of these mixtures is in the range of a few micrometers. From the voltage-transmission curves shown in Fig. 6, one can see that for CB15

concentrations up to approx. 4%, the homeotropic state is stable at zero field.

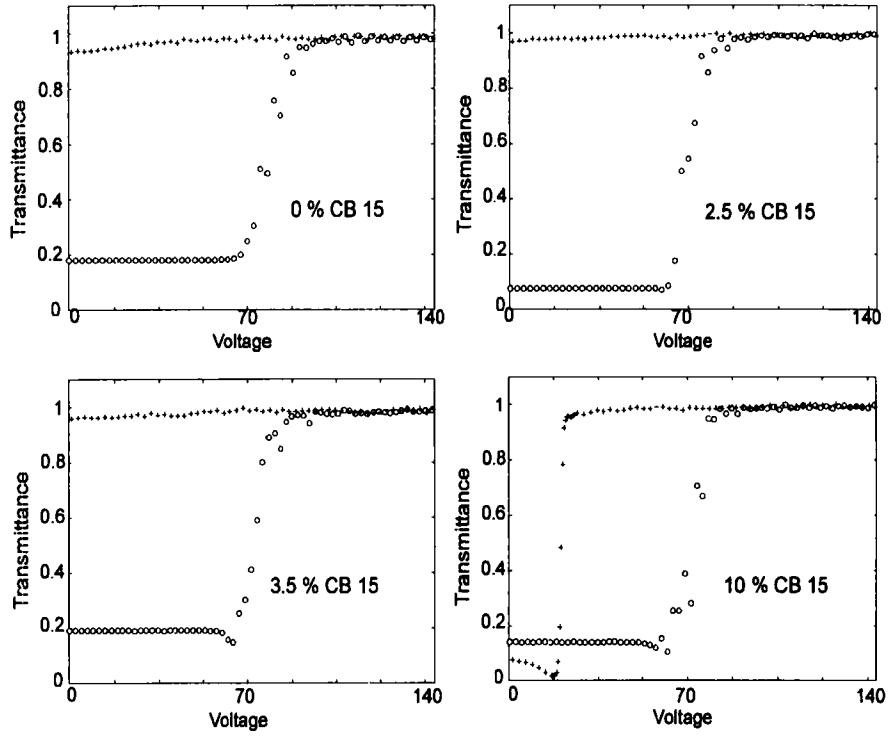

Figure 6: Voltage-transmittance curves for different chiral filled nematics (liquid crystal: ZLI-1132 (Merck), chiral dopant: CB15 (Merck), Aerosil: R974, 2.5 Vol%).

Now different samples of filled chiral nematics could be prepared to investigate their laser-writing properties.

Results

Fig. 7 shows the expected significant increase in sensitivity with the concentration of the chiral dopant. For example, with 4 % CB15 in the nematic liquid crystal E48 (BDH), the contrast ratio is more than doubled compared to a sample with pure E48 at the same absorbed laser energy. Such displays were used to improve the performance of the demonstration unit described in the introduction.

INFLUENCE OF BOUNDARY CONDITIONS: FILLED CHOLESTERICS

Further decreasing the pitch length of silica dispersed LCs, one might expect to obtain bistable textures similar to polymer stabilized cholesteric textures (PSCT), which were introduced recently by Yang and Doane[6]. PSCT displays can be

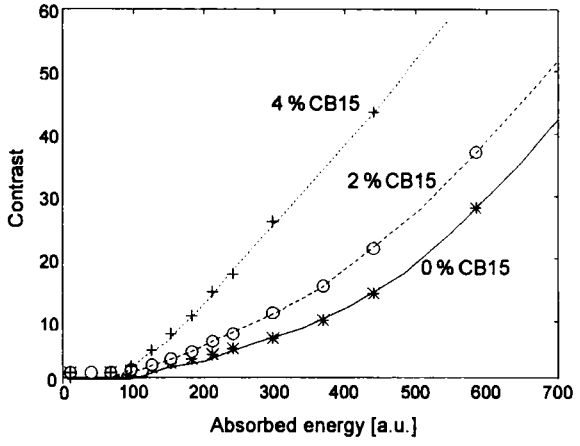

Figure 7: Results of laser writing in chiral filled nematics (liquid crystal E48, chiral dopant CB15, Aerosil: R974, 2.5 Vol%).

switched to either a planar Bragg-reflecting state or a weakly scattering focal conic state with pulses of different voltage.

We used dispersions of 1.5 Vol% Aerosil and a mixture of E48 with chiral components CB15 and CE1 reflecting green light to fabricate *filled cholesteric* cells of thickness of 3.2 μm and 7 μm.

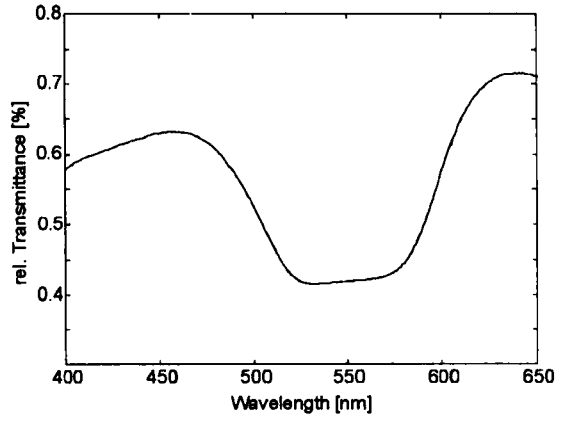

Figure 8: Transmittance of a filled cholesteric cell in the reflecting state; there is a broad reflection band around 550 nm.

Fig. 8 shows the transmittance of such a cell in the reflecting state as measured in a Perkin-Elmer Lambda 9 spectrometer. The cell shows a broadband diffuse reflection corresponding to a distribution of the helical axes around the direction perpendicular to the cell plates. The reflection bandwidth is comparable to the product of optical anisotropy and pitch length ($\Delta n \cdot p \approx 90$ nm).

Such properties make filled cholesteric cells suitable for direct view displays, since the reflection shows no strong dependence on the viewing angle.

Electrical switching

To investigate the static electro-optical behaviour of filled cholesterics (FC), we applied voltage pulses of 20 ms duration and measured the reflected intensity of a frequency-doubled Nd:YAG laser ($\lambda = 532$ nm) at an angle of 25 degrees. The result is shown in Fig. 9; the switching curves from transparent to reflecting state (and vice versa) look very similar to the curves obtained with PSCT[7].

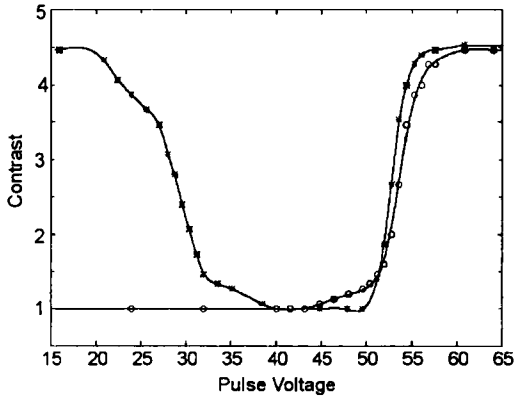

Figure 9: Static electro-optical behaviour of a filled cholesteric cell; o: switching from transparent to reflecting state, +: switching from reflecting to transparent and back to reflecting state.

Different boundary conditions

It is well known that the switching dynamics of PSCT crucially depend on the boundary conditions[8]. But comparing the dynamical behaviour of FC cells with planar surface conditions (polyimide coating) and without surface treatment, there seems to be no large difference. We applied two voltage pulses (40 V and 60 V) of 20 ms duration and measured the reflected intensity as a function of time with a Nd:YAG laser and photodiode as mentioned above. The results are shown in Fig. 10: The relaxation times for both states are almost equal for cells with and without polyimide coating.

A possible explanation is that applying the high voltage pulse leads a homeotropic state first[8], but here the relaxation to the planar state is controlled by the re-formation of the Aerosil structure rather than by boundary conditions.

The low voltage pulse drives the material into the focal conic state, which can also be stabilized by the network. The relaxation time is much shorter than for the planar state and the same for both cell types.

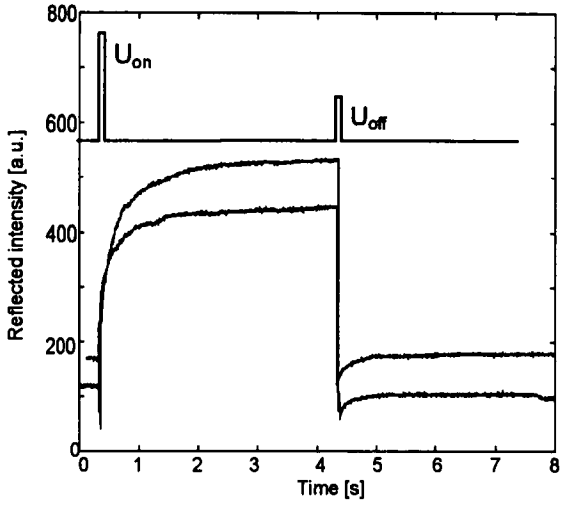

Figure 10: Dynamics of switching in filled cholesterics with polyimide layer (upper curve) and without polyimide layer (lower curve).

Laser writing in Filled Cholesterics

Differences turn up when the cells are laser-addressed using a setup similar to the system in Fig. 1 to write an image on the displays. Fig. 11 and Fig. 12 show photographs of two FC displays containing the same mixture, but having different surface treatment. The cells were placed in a microscope, with a black background and illumination from the top.

Obviously the display can be laser-addressed from the reflecting state to the transparent state without surface treatment. With a polyimide coating, the 'reverse mode' (laser writing from transparent to reflecting state) is possible.

This is a contradiction to the electro-optical measurements, where there was no influence on the switching dynamics from the boundary conditions. Laser writing experiments with PSCT have been carried out first by the Kent group, but only the transparent state was achieved[9].

To fully understand the effects described above, further investigations and theoretical considerations will be necessary, but the electro-optical and laser-addressing experiments with Filled Cholesterics can possibly help to gain further insight in the mechanisms which take place in silica dispersed liquid crystals.

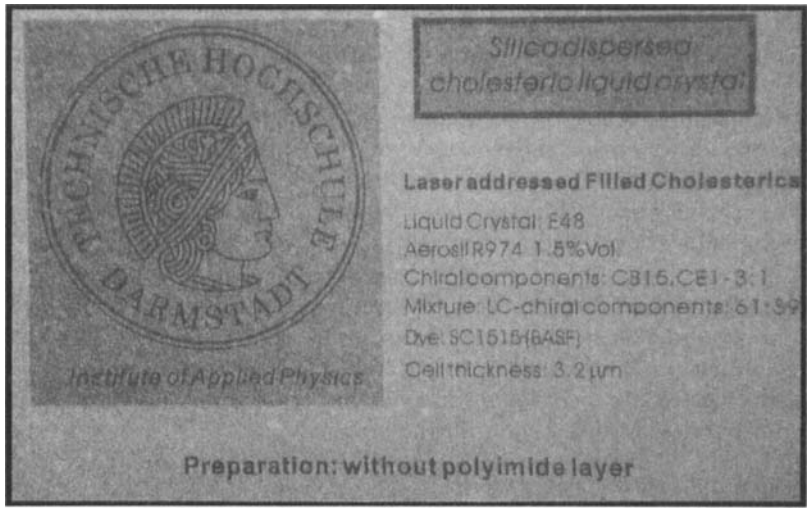

Figure 11: Photograph of a laser-written image in a filled cholesteric cell *without* polyimide coating. The original image size is 8 mm × 5 mm. See **Color Plate II.**

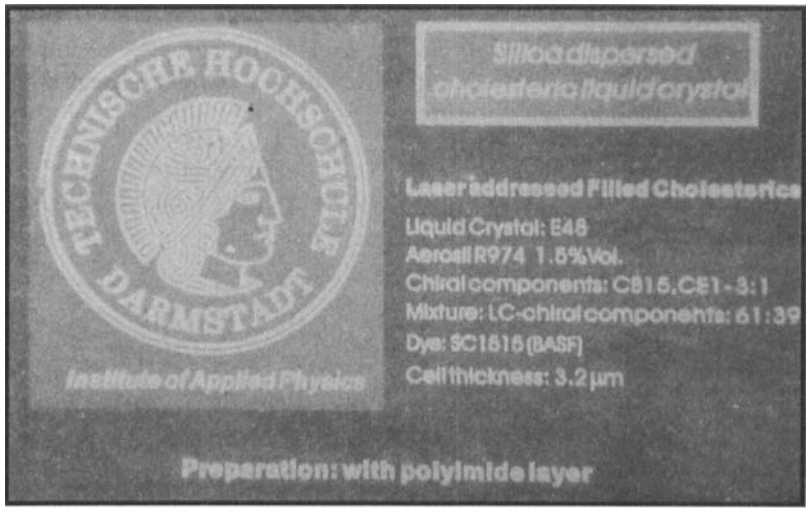

Figure 12: Photograph of a laser-written image in a filled cholesteric cell *with* polyimide coating. The original image size is 8 mm × 5 mm. See **Color Plate III.**

CONCLUSIONS

Filled Nematics are promising materials for projection display applications. Extremely high information content can be achieved with laser addressing. In order to understand and optimize the mechanism of laser writing in FN, we proposed a theoretical model which is confirmed by experimental observations.

With an understanding of the laser writing process, we have been able to enhance the sensitivity using chiral nematics and thus achieve higher writing speed. This was immediately utilized for application in a demonstration projection system.

Filled Cholesterics form bistable textures which can be electrically switched to transparent and reflecting states. Laser addressing is also possible to both states depending on the boundary conditions. The properties of this material give further clues to the mechanisms in silica dispersed liquid crystals and possibly open up the field of direct-view display applications.

REFERENCES

1. M. Kreuzer, T. Tschudi and R. Eidenschink, Mol. Cryst. Liq. Cryst. ,223, pp. 219-227 (1992)
2. A. G. Dewey, Opt. Eng., 23 (3), p. 230 (1984)
3. M. Kreuzer, T. Tschudi, W. H. de Jeu and R. Eidenschink, Appl. Phys. Lett., 62, pp. 1712-1714 (1993)
4. P. G. De Gennes, in The Physics Of Liquid Crystals (Clarendon Press, Oxford, 1974)
5. M. Kreuzer and R. Eidenschink, in Liquid Crystals in Complex Geometries Formed by Polymer and Porous Network, edited by G.P. Crawford and S. Zumer (Taylor & Francis, London, 1995), in press.
6. D.-K. Yang et al., Appl. Phys. Lett., 60 (25) , p. 3102 (1992)
7. D.-K. Yang et al., Appl. Phys. Lett., 64 (15) , p. 1906 (1994)
8. D.-K. Yang et al., J. App. Phys., 76 (2) , pp. 1331-1332 (1994)
9. T. Kosa and P. Palffy-Muhoray, private communication